Bioprinting 36 (2023) e00313

Contents lists available at ScienceDirect

Bioprinting

journal homepage: www.sciencedirect.com/journal/bioprinting

The 3D bioprinted human induced pluripotent stem cell-derived cardiac model: Toward functional and patient-derived *in vitro* models for disease modeling and drug screening

Henna Lappi [a,*], Maija Kauppila [b], Katriina Aalto-Setälä [a,c,1], Anni Mörö [b,1]

[a] *Heart Group, Faculty of Medicine and Health Technology and BioMediTech Institute, Tampere University, 33520, Tampere, Finland*
[b] *Eye Regeneration Group, Faculty of Medicine and Health Technology and BioMediTech Institute, Tampere University, 33520, Tampere, Finland*
[c] *Heart Hospital, Tampere University Hospital, 33520, Tampere, Finland*

ARTICLE INFO

Keywords:
3D bioprinting
Human induced pluripotent stem cells
Cardiomyocyte
Bioink
In vitro model
3D disease model

ABSTRACT

More relevant human tissue models are needed to produce reliable results when studying disease mechanisms of genetic diseases and developing or testing novel drugs in cardiac tissue engineering (TE). Three-dimensional (3D) bioprinting enables physiologically relevant positioning of the cells inside the growth matrix according to the detailed digital design. Here we combined human induced pluripotent stem cell (hiPSC)-derived cardiomyocytes (CMs) with methacrylated gelatin (GelMA) and collagen I-based bioink and 3D extrusion bioprinted a cardiac *in vitro* model for disease modeling and drug screening. Bioprinted constructs were characterized for their rheological properties, swelling behavior, degradation, as well as shape fidelity. The printed structures demonstrated good mechanical properties and high shape fidelity upon culture. Immunocytochemistry revealed elongated hiPSC-CMs growing inside the structures and the presence of the connexin 43 marker, indicating cardiac gap junctions between printed cells and tissue formation. Extensive functional analyses with calcium imaging showed normal functionality and calcium-handling properties for hiPSC-CMs. Finally, suitability of this 3D bioprinted construct for patient-specific disease modeling was demonstrated by bioprinting hiPSC-CMs from a patient carrying an inherited gene mutation causing catecholaminergic polymorphic ventricular tachycardia (CPVT). CPVT hiPSC-CMs responded to adrenaline treatment in the 3D bioprinted model in a manner that is characteristic for CPVT disease specific phenotype. Thus, the 3D bioprinted hiPSC-CM *in vitro* model has great potential for disease modeling and drug screening in cardiac tissue engineering.

1. Introduction

Cardiovascular diseases are the leading cause of mortality worldwide [1]. Primary treatment option for patients is a pharmacological approach which often has limited advantages. Besides of the need for better cardiac drugs, drug-induced cardiotoxicity is a severe complication and is not only the leading cause of failure of novel drugs in preclinical and clinical trials but also one of the leading causes (14 %) of the withdrawal of drugs (cardiac and non-cardiac) already on the market [2,3]. Additionally, a major limitation in drug development is the wide use of animals in preclinical studies, resulting in approximately 92 % failure of all drug compounds clinical trials mainly due to difficulties in translating results from animal-related studies into human treatments [4]. Rodents are often chosen as primary animal models for drug development mainly due to the overall cost-effectiveness and short gestation time [5]. However, there are major differences in human and animal cardiac physiological parameters such as the beating rate, response to the increase in beating rate during exercise, expression of various protein isoforms, as well as the shape of action potentials [6]. Therefore, human-based models are desperately needed to have more reliable and predictive tools for drug discovery and screening applications. These models can be used not only for faster and safer drug development but also for studying disease mechanisms, structural and functional phenotypes, and the effects of various gene mutations [7,8].

Cardiac tissue engineering (TE) provides an alternative tool to study cardiovascular diseases and its main objective is to recapitulate the

* Corresponding author.
E-mail address: henna.lappi@tuni.fi (H. Lappi).
[1] Equal contribution.

https://doi.org/10.1016/j.bprint.2023.e00313
Received 21 June 2023; Received in revised form 22 September 2023; Accepted 5 October 2023
Available online 9 October 2023

physiological tissue environment to enable investigations of cardiac muscle function and biology under both physiological and pathological conditions [9,10]. Human induced pluripotent stem cells (hiPSCs) have emerged as a key tool of cardiac TE, enabling studies of cardiovascular disease mechanisms, drug responses, and developmental processes in human 3D tissue models [9]. Today, researchers have relatively easy access to patient-derived hiPSCs, enabling the modeling of structural and functional inherited genetic cardiac conditions such as catecholaminergic polymorphic ventricular tachycardia (CPVT) [11], hypertrophic cardiomyopathy [12], or long-QT syndrome [13,14]. It has previously been demonstrated using hiPSC cardiomyocyte (hiPSC-CM) models that the 3D environment enhances functionality and maturation compared to their two-dimensional counterparts [15,16]. In the future, the 3D culture of hiPSC-CMs opens opportunities for achieving tissue models that replicate more closely native physiological conditions [17–21].

3D bioprinting has several advantages over traditional biofabrication technologies, including full control over the shapes and compositions of their printed components as well as the precise placement of diverse cell populations throughout the entirety of the construct, providing a powerful tool to manufacture precise 3D cardiac models [22]. In a human heart, cardiomyocytes are highly oriented and grow spatially in contact with other cells and the extracellular matrix (ECM) [14,23]. Orienting the CMs in cell culture requires guiding element such as suitable biomaterial, grooves or filaments [24]. As seen in most of the CM bioprinting studies, it is difficult to adequately and uniformly control the microstructure and individual cell placement within the constructs with the spheroid approach [25–28] or in methods where the cell laden bioinks are seeded without any additional guidance [22,29]. Only two previous studies have reported 3D bioprinting of hiPSC-CMs using photocrosslinkable gelatin based bioinks to orientate hiPSC-CMs in 3D constructs [30,31]. Previously, hiPSC-CMs have been 3D bioprinted with extrusion printing merely to demonstrate the possibility of utilizing these more sensitive cells in bioprinting while biocompatibility analyses in these studies are performed with more robust cell types of animal origin such as primary or rat CMs [30,32,33]. Calcium (Ca^{2+}) is a key factor in CM excitation-contraction coupling and abnormalities in Ca^{2+} handling can cause arrhythmias. Imaging of Ca^{2+} fluxes (Ca^{2+} imaging) in CMs can be used for studying these mechanical properties [34]. In our previous study, we demonstrated adrenaline-induced Ca^{2+} abnormalities in CPVT hiPSC-CMs in 2D conditions [11]. To the best of our knowledge, the functionality of diseased patient-derived CPVT hiPSC-CMs has not been previously explored in 3D bioprinted structures. Despite the recent progress in the field, technological breakthroughs are needed to unleash the full potential of 3D bioprinting for cardiac TE and to shift the paradigm toward functional hiPSC-based disease models.

Bioinks for cardiac tissue constructs should form *in vivo*-mimicking microenvironments for the cells, which should be biocompatible, printable, and stable in culture [35]. Cardiac ECM is composed of proteins, with collagens (type I collagen accounting for 80 %) being the most prominent group [36]. Collagens and collagen-based scaffolds also provide important functional benefits in that they provide an abundance of native heart-like ligands to embedded cells and promote the cell-mediated remodeling of tissue architecture [9]. GelMA is an appealing hydrogel to be utilized in bioprinting in many ways such as photocrosslinking in the presence of photoinitiators such as lithium phenyl-2,4,6-trimethylbenzoylphosphinate (LAP) [37]. Previously, both of these bioink components, GelMA [38] and collagen I [39], have been used in cardiac applications either as such or in combination with other polymers. However, the use of blends of GelMA and Collagen I-has not been previously reported for 3D bioprinting of hiPSC-CMs.

In this study, we addressed these challenges by 3D bioprinting functional hiPSC-derived cardiac *in vitro* model. hiPSC-cardiomyocytes were printed in GelMA and collagen I-based bioink with extrusion printing. Herein, we demonstrated that 3D bioprinted structures have high shape fidelity and good mechanical properties. Moreover, hiPSC-CMs inside the 3D-printed structures showed more physiologically relevant and elongated cell morphology than their 2D counterparts. Cardiomyocyte functionality in the bioprinted 3D *in vitro* model was assessed with extensive Ca^{2+} imaging experiments with healthy and diseased patient-derived hiPSC-CMs. Here, we demonstrated the feasibility of the 3D bioprinted hiPSC-CM for cardiac TE applications including drug screening and disease modeling.

2. Materials and methods

2.1. Human induced pluripotent stem cell derived cardiomyocytes

A healthy human iPSC line, UTA.D103-4 [40], and a patient-specific iPSC line, UTA.05503.CPVT [11], were used. The control cell line was obtained from a healthy female and the patient-specific cell line was derived from a female individual carrying a RyR2 mutation (Q4201R). The patient had CPVT, which causes exercise-induced ventricular arrhythmias. The donors gave their written informed consent. The study was approved by the Pirkanmaa Hospital District ethical committee (R08070).

hiPSC lines were cultured on the Geltrex LDEV-free hESC-qualified reduced growth factor basement membrane matrix (Geltrex, Gibco, Thermo Fisher Scientific, Massachusetts, USA) diluted 1:100 to DMEM/F12 (DMEM/F-12, Gibco, Thermo Fisher Scientific). hiPSCs were cultured in the mTeSR1 medium (Stemcell Technologies, Vancouver, Canada) supplemented with 50 U/ml Penicillin/Streptomycin (Pen/Strep, Lonza, Gampel-Bratsch, Switzerland) and passaged every 7 days via treatment with Versene (Gibco, Thermo Fisher Scientific).

hiPSC-CMs were differentiated via the embryoid body (EB) method as previously reported [41]. Briefly, hiPSCs were detached by Versene (Thermo Fisher Scientific) and seeded on ultra-low attachment 6-well plates (Corning, Massachusetts, USA) in the mTeSR1 medium supplemented with 5 μM Blebbistatin (Sigma-Aldrich, Missouri, USA) to enhance EB formation. From differentiation day 1 onward, EBs were cultured in the differentiation medium containing the RPMI 1640 medium (Gibco, Thermo Fisher Scientific), B-27 minus insulin (B-27-ins, Gibco, Thermo Fisher Scientific), and 50 U/ml Pen/Strep. First, the differentiation medium was supplemented with 5 μg/ml L-ascorbic acid 2-phosphate sesquimagnesium salt hydrate (Sigma-Aldrich), 10 ng/ml BMP4 (R&D Systems, Minneapolis, USA), and 25 ng/ml Activin A (Peprotech, Cranbury, USA) on day 1. Supplements were removed on day 3 and on day 4 2.5 μM IWP-4 (Tocris Bioscience, Bristol, UK) was added to the refreshed differentiation medium and removed on day 8. The medium was refreshed every other day and from day 10 onward, the medium was changed to a maintenance medium containing the RPMI 1640 medium with the B-27 supplement (Gibco, Thermo Fisher Scientific) and Pen/Strep.

For 3D bioprinting, beating hiPSC-CM clusters were dissociated as single cells at day 23–44 of differentiation either by collagenase A (Roche, Basel, Switzerland) [42] or by Multi Tissue Dissection Kit 3 (Miltenyi Biotech, Bergich Gladbach, North Rhine-Westphalia, Germany). Single hiPSC-CMs were suspended in a 20 % FBS medium containing fetal bovine serum (FBS, Sigma-Aldrich), Knockout-DMEM (KO-DMEM, Gibco, Thermo Fisher Scientific) supplemented with 1 % non-essential amino acid (NEAA, Lonza), 2 mM GlutaMax (Gibco, Thermo Fisher Scientific), and 50 U/ml Pen/Strep. Bioink was prepared by combining one part of the cell suspension with nine parts of GelMA bioink with 0.25 % LAP (Cellink, Gothenburg, Sweden) and a final concentration of 0.6 mg/ml of collagen I (OptiCol Human Collagen Type I, Cell Guidance Systems, Cambridge, UK). The concentration of the LAP photoinitiator in the final bioink was 0.21 %. Cell concentrations of 4.0–15.3 million cellsml^{-1} were used in bioprinting experiments for live/dead analyzes, stainings and for Ca^{2+} imaging. In acellular bioprintings, the 20 % FBS medium was used instead of a cell suspension.

Magnetic-activated cell sorting (MACS) was performed for differentiated CPVT hiPSCs directly after dissociation to purify the CMs. The

PSC-Derived Cardiomyocyte Isolation Kit, human (Miltenyi Biotec), was used for MACS sorting according to manufacturer's instructions. MACS-sorted CPVT hiPSC-CMs were mixed with bioink in a concentration of 4.0 million cellsml^{-1} and proceeded to 3D bioprinting.

2.2. Optimizing 3D bioprinting

The fabrication of 3D structures was done with the extrusion bioprinter 3D-Bioplotter Manufacturer Series by Envisiontec (Gladbeck, Germany). The printhead was preheated to +32 °C and 32G needles with 100 μm inner diameter were chosen (Cellink). The printing platform was cooled down to 10 °C. Twelve different bioprinting conditions were evaluated to optimize bioprinting to shape fidelity with the used bioink composition. Pressures ranging from 0.4 bar to 0.7 bar and speeds of 8 mm/s, 12 mm/s, and 16 mm/s were tested. Images of each printed layer were taken with a 3D Bioplotter camera. The printed structures were stabilized by photocrosslinking with UV. For this, each bioprinted layer was exposed to UV at 365 nm wavelength by using a 10 mm spot diameter, at a 30 mm distance with a speed of 6 mm/s. Structures were stabilized for 5 min at room temperature before washing with phosphate buffered saline (PBS, Lonza) to remove uncrosslinked GelMA. Thereafter, the printed samples were cultured at 37 °C and 5 % CO_2 in a 20 % FBS medium supplemented with Y-27632 dihydrochloride (ROCK inhibitor, Tocris). The ROCK inhibitor was removed after 24 h. Cell-laden structures were cultured for a maximum of 14 days and acellular structures for up to 20 days.

To support visual evaluation of filament structures formed with different printing conditions, images from all twelve printing conditions taken after printing of second layer were analyzed with ImageJ plugin TWOMBLI [43] and were compared to analysis results from computer modelled grid. Analysis was done with fixed parameters of contrast saturation of 0.350, line width of 40, curvature 400, and minimum branch length of 20. Seven parameters (lacunarity, total length of filaments, endpoints, branchpoints, fractal dimensions, curvature, and alignment) were analyzed from the images and were scored according to their correspondence to results from computer modelled grid, two most similar results from each category received one point and two least similar were decreased by one point. Endpoint and branchpoint data were normalized to total length of the filaments as recommended in an article from Wershof et al. [43].

Three different bioprinted structures were bioprinted according to their purposes of use. Bioprinted lattice structures were three-layered, square-shaped either 20 × 20 mm or 10 × 10 mm with a 1 mm distance between parallel lines and with 80 μm slice intervals. Cell-laden constructs were used for hiPSC-CM characterizations and acellular samples for filament stability studies. Bulk samples were bioprinted as seven-layered, 600 μm thick, round lattice structures with 0.3 mm distances between parallel lines and subsequently used for material analysis studies. For immunofluorescence staining and Ca^{2+} imaging 10 × 10 mm structures were printed on glass bottom dishes (MatTek Corporation, Massachusetts, USA) and on 12 mm ø glass coverslips (VWR Collection, Pennsylvania, USA). For other analysis, structures were printed onto 3.5 cm cell culture dishes (Nunc, Thermo Fisher).

2.3. Characterization of the bioink and bioprinted structure

2.3.1. Swelling and physical degradation

The hydration of the bioprinted structures was studied in a swelling experiment to predict material behavior during the post-printing culture period. Samples for degradation and swelling studies were triplicate bulk samples that were weighted and imaged after a 30-min stabilizing stage (0h) at nine time points from 0 h to 20 days. Samples were cultured either in DPBS or in the 20 % FBS medium in an incubator at 37 °C and 5 % CO_2. Accelerated enzymatic degradation was studied to be able to predict material degradation. After a 30-min stabilization the structures were treated with 0.375 mg/ml collagenase type I (Gibco) in the Ko-DMEM medium. Images were taken and structures were weighted at five timepoints during the 2-h culture period in which the whole structure was completely degraded. Structures in Ko-DMEM media were used as controls. Results are reported as the relative weight (normalized to the original weight) progresses during the follow-up period.

2.3.2. Filament stability

The stability of the filaments was studied to evaluate changes in fabricated filaments during the extended culture period. Triplicate acellular 20 x 20 lattice structures were imaged with 4x, 10x, and 20x magnification with the Nikon Eclipse TS100 (Nikon Corporation, Tokyo, Japan) microscope with an attached DIGI-12 (Optika, Bergamo, Italy) camera at four time points up to 7 days post-printing. The widths of the first layer filaments were measured from the images in each time point from a total of 78 points using ImageJ software. The number of pixels was converted to the corresponding μm value per the used magnification.

2.3.3. Rheology

Viscoelastic properties of bioprinted and acellular structures were characterized by rheological measurements. Samples were cultured for 24 h in a culture medium and oscillatory measurements were conducted using the Discovery Hybrid Rheometer-2 (DHR-2, TA-instruments, New Castle, USA) at 25 °C utilizing 20 mm diameter parallel-plate geometry. Measurements were conducted from four replicates. An oscillatory frequency sweep was performed within the liner viscoelastic region (0.1–20 Hz at 1.6 % shear strain) to determine storage (G′) and loss (G″) moduli of photo-cured structures.

2.4. Characterization of bioprinted human induced pluripotent cardiomyocytes

2.4.1. Cell viability

Cell viability was assessed from the bioprinted samples 24 h post-printing by staining all nuclei with the NucBlue™ live reagent (ReadyProbes Cell Viability Imaging Kit, Invitrogen, Thermo Fisher Scientific) while 0.1 μM Calcein-AM (Invitrogen) was applied to stain live cells. 2D control samples were prepared from the same dissociation batch as the cells that proceeded to 3D bioprinting. Control samples were plated on 0.1 % gelatin coated wells in EB medium, as in standard cell culture. After 24 h, NuncBlue™ (Thermo Fisher Scientific) and Calcein-AM (Thermo Fisher Scientific) were added to the wells and cells were imaged. From combined images, the co-expression of green and blue fluorescence (Calcein-AM green excitation/emission 488/515 nm, NucBlue blue excitation/emission 504/523 nm) indicated live cells whereas the expression of solely blue (NucBlue) indicated dead cells. Stained samples were imaged with 10x magnification on an EVOS fluorescent microscope (Invitrogen). Single-channel images were analyzed using the ImageJ particle analysis which counted stained areas from Calcein-AM and NuncBlue stained images that were further compared to calculate the viability percentage.

2.4.2. Immunofluorescence staining

The hiPSC-CM morphology and migration in 3D bioprinted constructs were analyzed via immunofluorescence staining. Samples were fixed with 4 % paraformaldehyde on day 8 or 14 post-printing, permeabilized with 0.1 % TritonX-100, blocked with 10 % normal donkey serum (NDS, Biowest, Nuaillé, France) and 1 % bovine serum albumin and incubated for 2 days with primary antibodies for cardiac troponin T (1:1000), and connexin 43 (1:800, all reagents form Sigma-Aldrich except NDS). For secondary antibodies, Alexa fluor 568 IgG anti-mouse (1:500, Thermo Fisher Scientific) and Alexa fluor 488 IgG anti-rabbit (1:500, Thermo Fisher Scientific) were applied overnight. All the cells in the samples were stained with phalloidin 568 (1:100, Molecular Probes) and nuclei with 0.2 μg/ml DAPI (Sigma-Aldrich). Images were taken with an IX51 Olympus inverted fluorescence microscope

(Olympus, Tokyo, Japan), Axio Scope 1A inverted fluorescence microscope (Carl Zeiss, Jena, Germany), or Zeiss LSM 800 confocal microscope (Carl Zeiss).

2.4.3. Calcium imaging of hiPSC-CMs

The functionality of 3D bioprinted hiPSC-CMs was explored by assessing the Ca^{2+} handling properties after 7 days of culture. 3D and 2D control samples for hiPSC-CM measurements were from two separate differentiations and bioprinting experiments where total of seven 3D bioprinted samples (n = 7) and six 2D control samples (n = 6) were prepared. All CPVT hiPSC-CM 3D and 2D control samples were from the same differentiation and bioprinting. Total of five 3D samples (n = 5) and seven 2D samples (n = 7) were prepared. All CMs for Ca^{2+} imaging were cultured 36 days prior the bioprinting. The CMs in 3D bioprinted samples and 2D controls on 0.1 % gelatin-coated cover slips were loaded with 6 μM Fluo-4 AM (Invitrogen) for 40 min in an extracellular solution containing (in mM) 137 NaCl, 5 KCl, 0.44 KH_2PO_4, 20 HEPES, 4.2 $NaHCO_3$, 5 D-glucose, 2 $CaCl_2$, 1.2 $MgCl_2$ and 1 Na-pyruvate with an adjusted pH of 7.3. The spontaneous beating of hiPSC-CMs was imaged with 20x magnification on an Axio 1A inverted fluorescence microscope (Carl Zeiss) equipped with an ANSOE iXON3 camera (Andor Technology, Belfast, UK). Imaging was done on a +37 °C heat-plate with Filter Set 46 HE (Zeiss, excitation-emission wavelength of 494/516 nm). Total of 58 measurements from 3D hiPSC-CMs were analyzed. Analyzed videos were 30 s long and were imaged using a framerate of 34 frames/second. For Ca^{2+} imaging analyzes, the region of interest was defined from the hiPSC-CMs, and background fluorescence was subtracted from the data before further analyzes. Imaging data were analyzed using Clampfit software (Molecular Devices, California, USA). In the CPVT hiPSC-CM part of the study 2D and 3D bioprinted samples were treated with 1 μM of adrenaline (Sigma-Aldrich, diluted in sterile H_2O). After baseline measurement, CPVT hiPSC-CMs were incubated with adrenaline for 5 min before recording of Ca^{2+} transients.

2.5. Statistical analysis

Statistical significance for degradation studies was determined via the Friedman test. The Kruskal-Wallis test, followed by Dunn's test, was applied for filament stability data. The statistical significance of the differences between the two groups in enzymatic degradation and Ca^{2+} imaging was evaluated using the unpaired *t*-test. $p < 0.05$ was considered statistically significant and levels of significance are presented as (*) $p < 0.05$, (**) $p < 0.01$ and (***) $p < 0.001$. Data are expressed as the mean ± S.E.M. and n refers to the number of cells or experiments.

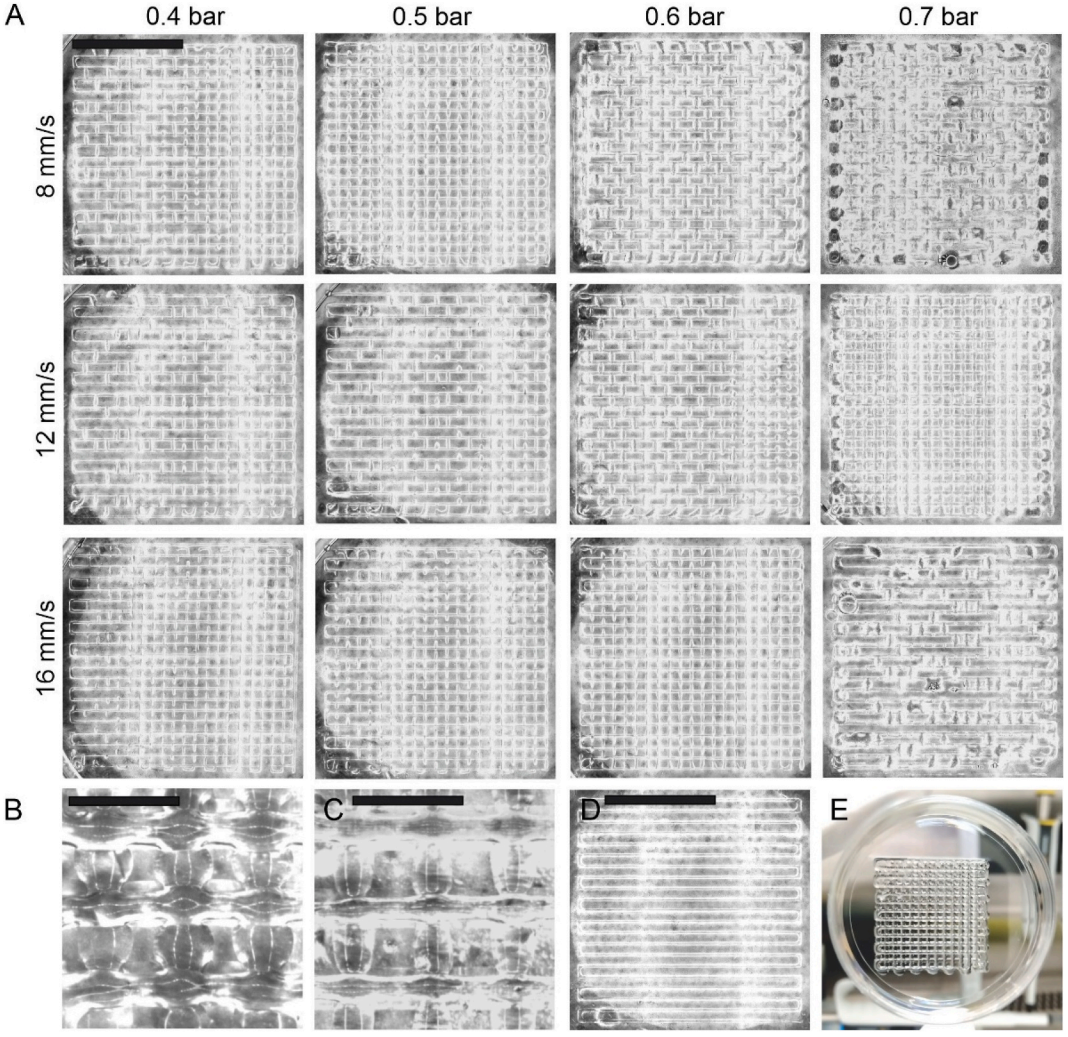

Fig. 1. Optimization of the bioprinting parameters of the GelMA and collagen I-based bioink for hiPSC-CM printing. (A) High-definition images taken immediately after printing for the evaluation the printing quality with different printing parameters. Scale bar 1000 μm. (B) High magnification images of the printed filaments with the highest (B, 0.7 bar and 16 mm/s) and (C) lowest (C, 0.4 bar and 8 mm/s) parameters. Scale bars B and C 50 μm. (D) Exemplary image of the first printed layer of planar lattice printed with 0.5 bar pressure and 8 mm/s speed, scale bar 1000 μm. (E) hiPSC-CM containing 3D bioprinted, three layered, lattice structure on a cell culture dish.

3. Results

3.1. GelMA and collagen I-based bioink show good printability and stability

Initially, we optimized the bioink composition and printing parameters for the bioink. Several printing parameters were explored in search of constructs resembling the original digital lattice design composed of filaments. To achieve this, key printing process parameters for extrusion-based bioprinting including printing pressure and speed, were adjusted. Clear differences were detected in the printability of the bioink with different parameters (Fig. 1A). The differences in printing quality and shape fidelity were the most distinguishable in perpendicular filaments in printed planar lattice structures with two layers. Printing pressures of 0.6 and 0.7 bars resulted in filament thickness increments (Fig. 1B). When lower printing pressures of 0.4 and 0.5 bars were applied, the formed filaments were finer and stayed apart from the parallel filaments forming the desired lattice structure (Fig. 1C). With all investigated parameters, the first layer showed good printability (Fig. 1D). However, discontinuous and nonuniform filaments were detected with the second layer, especially when lower printing pressures and high speeds were used. The best filament formation, filament homogeneity, and uniformity were achieved with 0.5 bar and 8 mm/s. To support visual evaluation, second layer images from twelve printing parameters were analyzed with ImageJ plugin TWOMBLY. Analysis results from seven categories were scored resulting highest score to 0.5 bar and 8 mm/s and lowest score to 0.5 bar and 12 mm/s (Supplementary Figure 1). Therefore, the former parameters were chosen for further analyses and 3D bioprinting of hiPSC-CMs (Fig. 1E).

3.2. Operational stability and mechanical properties of the 3D bioprinted constructs

To confirm the suitability of the bioink and printed structures for an *in vitro* cardiac model, we carried out extensive analyses of their stability and mechanical properties. First, we measured the weight of the printed acellular samples kept in PBS or in a cell culture medium up to 20 days to verify the stability of the constructs in *in vitro* culture conditions. The weight of the printed constructs in the cell culture medium increased by 89 % from dry weight (0.063 g) during the initial 0.5-h swelling period; however, in PBS, the increase in weight was 47 % (from 0.098 g to 0.144 g) (Fig. 2A). Thereafter, the swelling leveled out as seen via the constant weight of the printed constructs in PBS reported during the 20-day follow-up period (Fig. 2A (blue line)). A slight decrease in the sample weight was detected in the cell culture medium after 72 h; however, this decrease was not statistically significant (Fig. 2A (orange line)). The weights and images of the printed constructs during the extended culture period enabled the prediction of possible geometrical and mass-related changes due to the degradation or swelling of the material. To analyze the shape fidelity upon culture, we quantified the filament thickness from printed planar latices immediately after printing and during the 7-day period post-printing (Fig. 2B). Immediately after printing, the filament thickness was 281.22 ± 8.12 µm. A slight increase in the filament thickness was detected during the first days post-printing with a thickness of 296.38 ± 8.49 µm on day 2 and 303.45 ± 7.57 µm on day 3. This is in line with the swelling seen with the larger printed structures in (Fig. 2A). The mean filament thickness reduced to 231.46 ± 22.30 µm on day 7. P remainings of uncrosslinked GelMA as well as the collagen type I used as a rheological modifier dissolve slowly away from the printed structures, potentially causing this reduction in the filament thickness day 7. Enzymatic degradation studies with collagenase I showed that acellular 3D printed constructs with an average initial weight of 145 mg degraded in 2 h (Fig. 2C (orange line)). Similar samples without exposure to enzymatic treatment showed no decrease in weight (Fig. 2C (blue line)). We also measured the viscoelastic properties of the GelMA and collagen I-based bioink via rheological

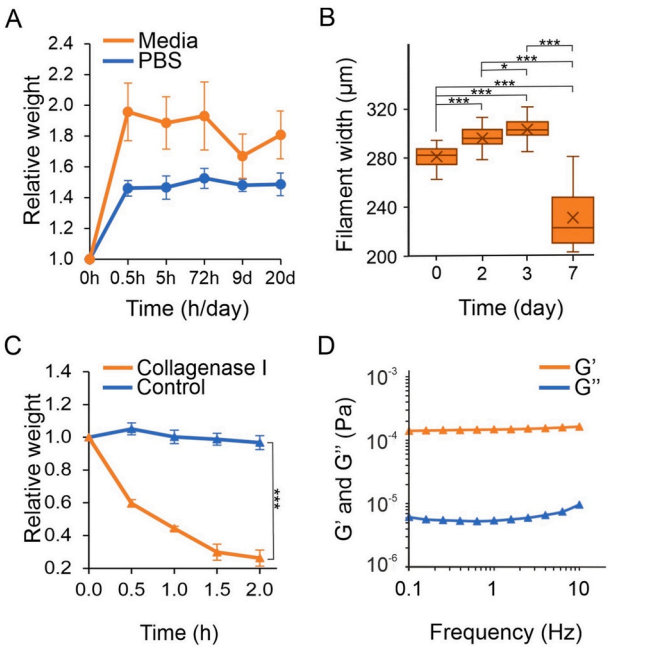

Fig. 2. Structural characterization of the GelMA and collagen I bioink and the printed constructs without cells. (A) Swelling and degradation of the printed constructs in cell culture media and PBS (n = 4 bioprinted samples). (B) Development of filament thickness and stability during 7-day culture (78 measuring points from 3 bioprinted samples). (C) Enzymatic degradation of the 3D printed constructs in collagenase I solution (n = 3 bioprinted samples). (D) Frequency sweep determined changes in storage modulus and loss modulus in constant 1.6 % strain (n = 4 bioprinted samples). $P < 0.05$ was considered statistically significant and levels of significance are presented as (*) $p < 0.05$, (**) $p < 0.01$ and (***) $p < 0.001$.

measurements. An oscillating amplitude sweep was performed to determine the maximum strain (1.6 %) within the linear viscoelastic region. A frequency sweep was performed with a constant 1.6 % strain from 0.1 Hz to 10 Hz. GelMA and collagen I-based bioink exhibited stable, gel-like behavior (G'>G″) with a mean storage modulus of 0.15 ± 0.018 kPa within the whole frequency region (Fig. 2D).

3.3. Characterization of hiPSC-CMs in the 3D bioprinted in vitro model

The bioprinted structures were characterized for cell viability, morphology, tissue formation, and functionality after bioprinting to demonstrate the feasibility of the method for creating 3D *in vitro* models with hiPSC-CMs. Live/dead analyses 24 h post-printing demonstrated good cell viability with 72 % live cells after printing (Fig. 3A). To compare, cells seeded onto 2D controls had a viability rate of 74 % (Fig. 3B). These data indicate that neither the printing process nor the bioink significantly hampers the cell viability of hiPSC-CMs in this setting. hiPSC-CMs showed rounded cell morphology 2 days post-printing (Fig. 3C and D). However, after the 7-day culture period, hiPSC-CMs had gained elongated cell morphology in the printed *in vitro* models (Fig. 3E and F). hiPSCs also demonstrated good cell proliferation and migration out of the printed filaments as seen in representative images of day 2 (Fig. 3C) and day 7 (Fig. 3G). Moreover, 3D bioprinted cardiac *in vitro* models were immunofluorescence (IF)-stained against phalloidin to visualize the cellular cytoskeleton, cell orientation, migration, and tissue formation (Fig. 4, images A, B, C). hiPSC-CMs were highly oriented in filaments of the lattices whereas, in filament intersections, cells showed a more random organization. Cardiac Troponin T was used to track the presence of hiPSC-CMs in 3D bioprinted samples (Fig. 4D, E and 4F). During visual inspection, hiPSC-CMs were nicely oriented with the filaments; however, at filament intersections, the

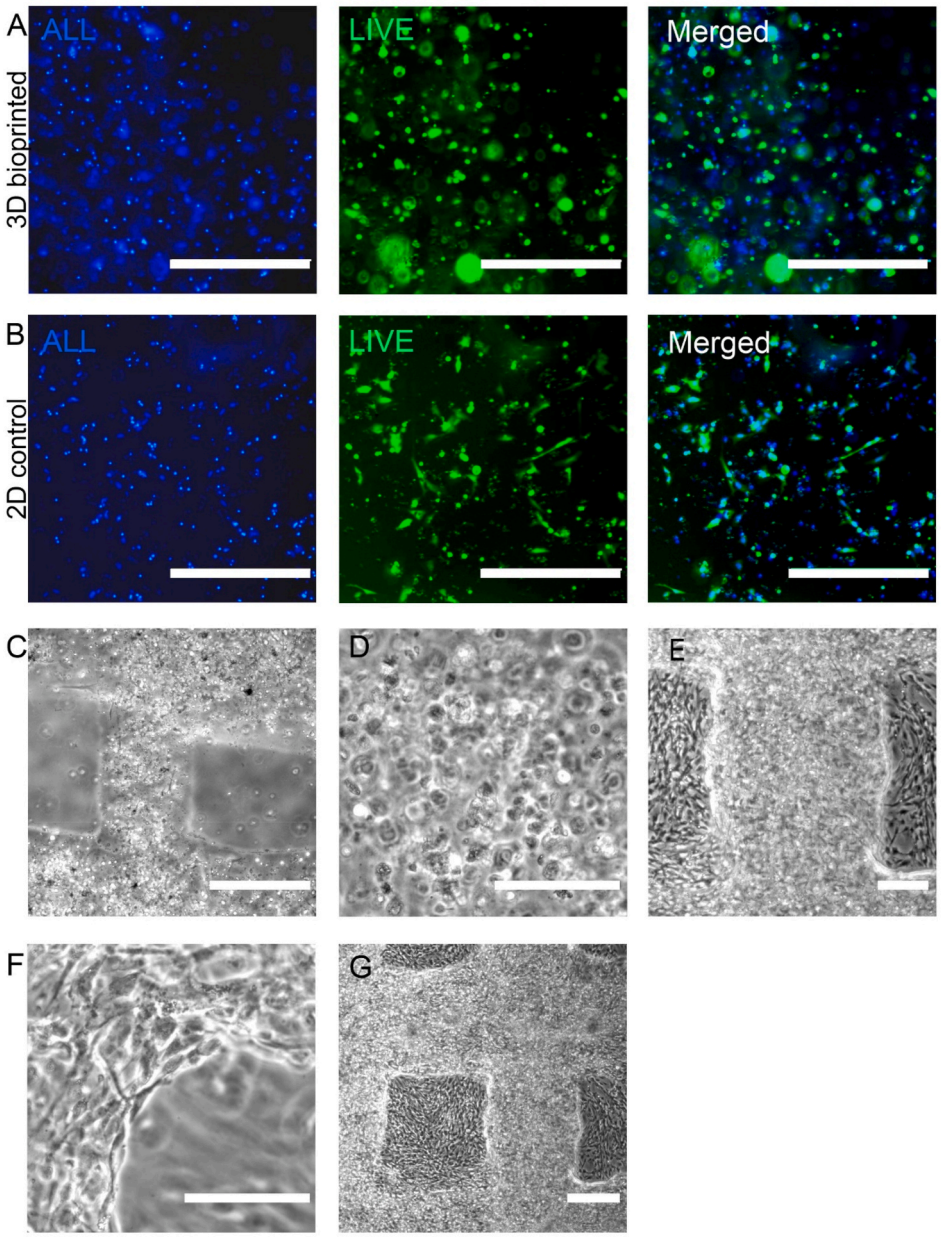

Fig. 3. Cell viability and morphology in the 3D bioprinted cardiac *in vitro* models. (A) Cell viability of hiPSC-CMs in the bioprinted 3D *in vitro* models 10x, scale bar 400 μm. Live cells are visualized with green. (B) Cell viability of hiPSC-CMs in 2D control 10x, scale bar 400 μm. (C) Phase contrast images of the 3D bioprinted *in vitro* models at day 2 post printing 4x, scale bar 400 μm (D) and on day 2 post printing 20x, scale bar 100 μm. (E) Phase contrast images of the bioprinted *in vitro* models at day 7 post printing 4x, scale bar 400 μm. (F) Day 7 post printing 20x, scale bar 100 μm. (G) Day 7 post printing 4x, scale bar 400 μm. (For interpretation of the references to colour in this figure legend, the reader is referred to the Web version of this article.)

orientation was lost. Images with higher magnification revealed highly elongated, branched cell morphology and oriented sarcomere structures (Fig. 4G, H and 4I). Larger image showing sarcomere orientation can be found from Supplementary Figure 2. A notable difference in hiPSC-CM cell morphology was observed between 3D bioprinted and 2D cultures (Fig. 4J). The hiPSC-CMs in 2D controls showed a round cell morphology with highly unorganized sarcomeres. hiPSC-CMs in 3D bioprinted *in vitro* models showed positive staining against the gap junction protein, connexin 43 (CNX), indicating the formation of cell-cell interactions and tissue formation post-printing (Fig. 4K). Interestingly, single CMs in the bioprinted *in vitro* models showed the expression of CNX closer to the nucleus (Fig. 4L).

3.4. Functionality of the 3D bioprinted hiPSC-CMs

The 3D bioprinted *in vitro* models showed beating hiPSC-CMs 15 days post-printing (Supplementary Video 1). The functionality of the 3D bioprinted hiPSC-CMs was studied further via Ca^{2+} imaging using the fluo-4 Ca^{2+} indicator. The Ca^{2+} kinetics of 3D bioprinted and 2D cultured hiPSC-CMs derived from a healthy individual were evaluated to study the effects of bioprinting and 3D culturing on the functional behavior of hiPSC-CMs. The beating frequency, in beats per minute (BPM), and the amplitude of the fluorescent signals relative to the baseline value (F/F0) were analyzed and compared between 3D bioprinted hiPSC-CMs and 2D controls. Our results showed that the averaged peak amplitude of 3D bioprinted hiPSC-CMs (2.0 ± 1.0 ($n = 7$)) was significantly ($p < 0.01$) higher than 2D controls (1.5 ± 0.7 ($n = 6$))

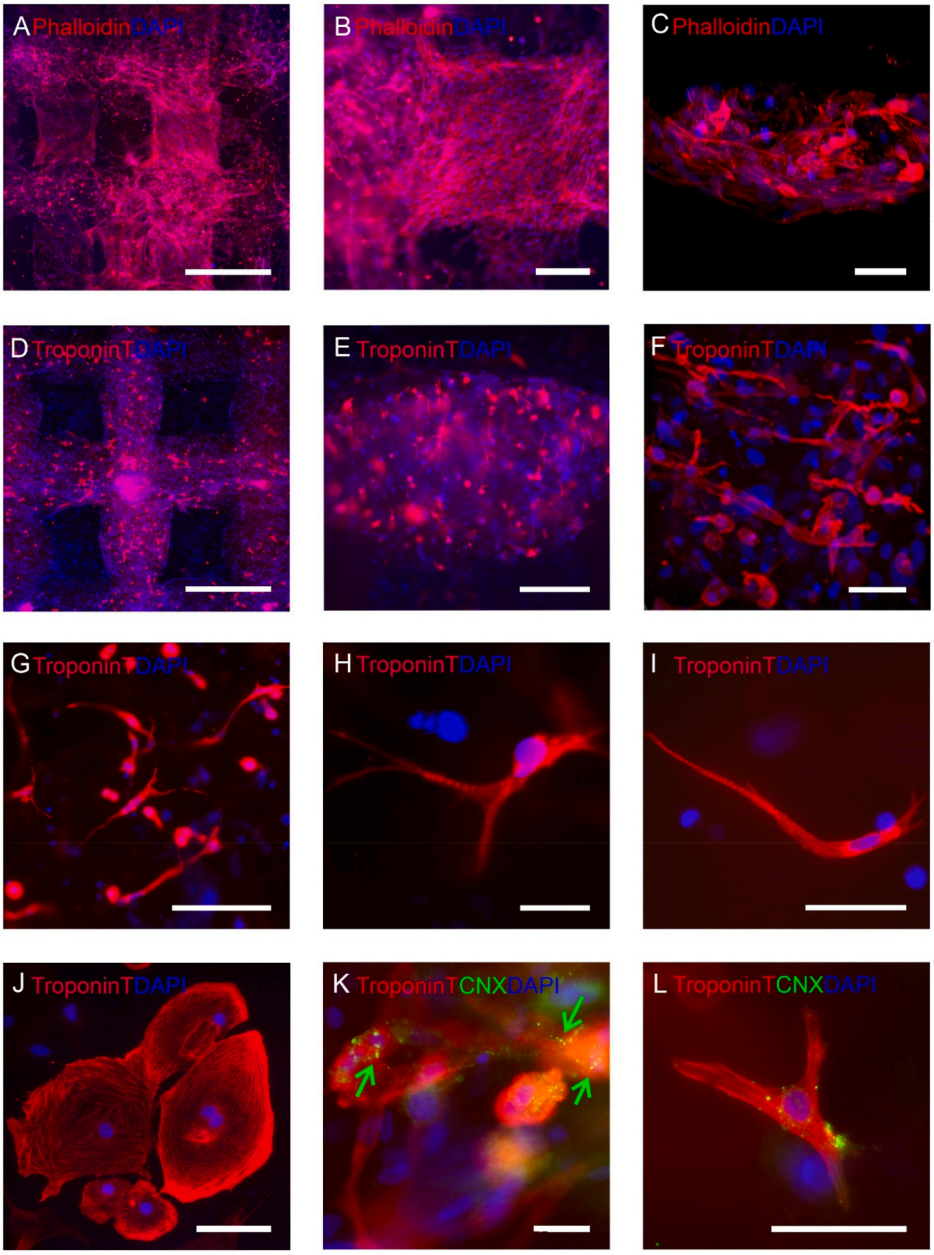

Fig. 4. Cardiac tissue formation after 3D bioprinting with hiPSC-CMs. (A) Representative low-magnification and (B) high-magnification images of immunofluorescence staining of phalloidin (red). Scale bars 1000 μm and 250 μm, respectively (C) Confocal maximum intensity projection image of phalloidin (red), scale bar 50 μm. D) Representative low-magnification and (E) high-magnification images of immunofluorescence staining of troponin T (red) in 3D bioprinted *in vitro* models with hiPSC-CMs 7 days post printing. Scale bars 1000 μm and 200 μm, respectively. (F) Confocal maximum intensity projection image of troponin T (red), scale bar 50 μm. (G–I) High-magnification images of the cell morphology and sarcomere organization scale bars, 250 μm, 25 μm and 50 μm, respectively. (J) Cell morphology and sarcomere structures in 2D controls, scale bar 100 μm. (K–L) Formation of cell-cell interactions in 3D bioprinted constructs was visualized with connexin 43 (CNX) (green). 3D bioprinted hiPSC-CMs demonstrated concentrated CNX expression between adjacent cells (marked with green arrows). Scale bars, 50 μm. The nuclei were visualized with 4′,6-diamidino-2-phenylindole (DAPI, blue). (For interpretation of the references to colour in this figure legend, the reader is referred to the Web version of this article.)

(Fig. 5B). Moreover, the mean beat rate of 3D bioprinted hiPSC-CMs (39 ± 22 (n = 7)) was significantly ($p < 0.001$) higher than that of 2D controls (11 ± 7 (n = 6)) (Fig. 5D).

Supplementary video related to this article can be found at doi:10.1016/j.bprint.2023.e00313

3.5. The 3D bioprinted CPVT hiPSC-CM in vitro model for disease modeling

In this final part of the study, we 3D bioprinted patient-specific hiPSC-CMs carrying CPVT mutation to demonstrate the proof of concept of the 3D *in vitro* model for cardiac disease modeling. For this, the patient-specific hiPSC-CMs were further MACS sorted to have only CMs present in these 3D bioprinted constructs. Ca^{2+} imaging was performed for CPVT hiPSC-CMs to evaluate the Ca^{2+} kinetics in the printed 3D environment. In addition, we also performed the adrenaline treatment to demonstrate drug molecules' (such as adrenaline's) ability to penetrate into GelMA collagen I-bioink. Clinically, the increased beating rate induces arrhythmias in CPVT patients. To recapitulate this clinical phenotype, adrenaline was used against CPVT hiPSC-CMs. The same

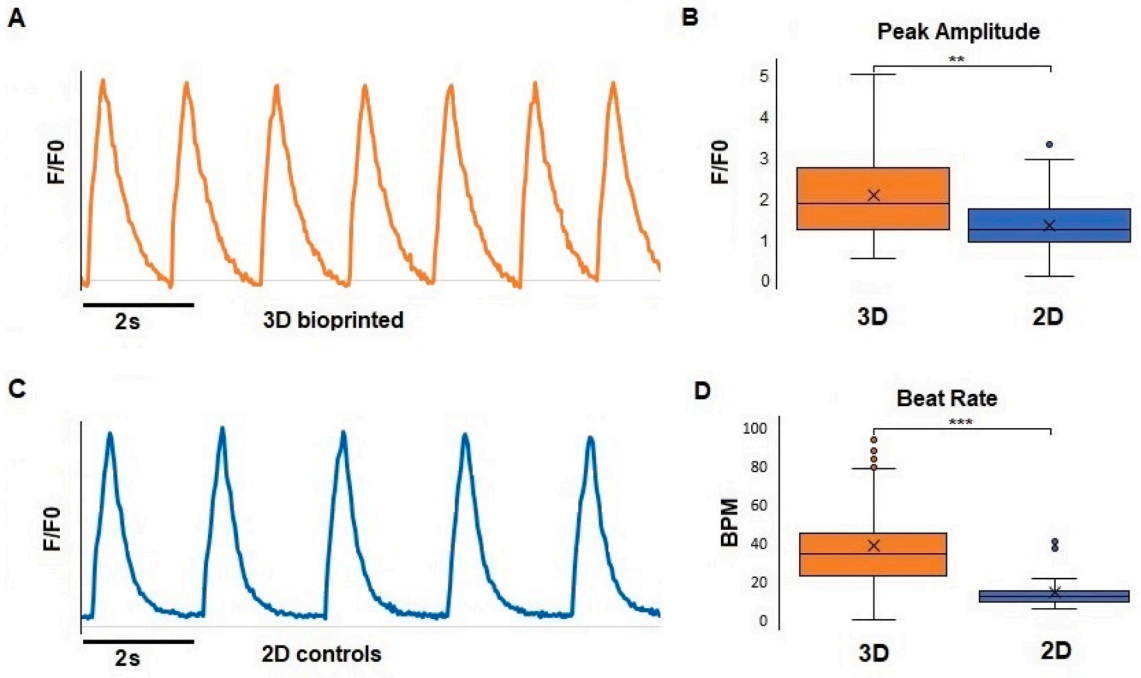

Fig. 5. Calcium activity of hiPSC-CMs in the 3D bioprinted *in vitro* model and in 2D controls. (A) Representative Ca^{2+} signal from 3D bioprinted hiPSC-CM. (B) Comparison of mean Ca^{2+} peak amplitude of hiPSC-CMs in 3D bioprinted (n = 7 3D bioprinted samples, in total of 58 measurement) samples and in 2D (n = 6 samples, 33 measurements) samples. (C) Representative image of Ca^{2+} activity of hiPSC-CMs in 2D sample. (D) Comparison of mean beating rate of hiPSC-CMs in the 3D bioprinted samples and in 2D controls (n = 6). All measurements were performed on day 7 after 3D bioprinting or dissociation and plating in 2D. $p < 0.05$ was considered statistically significant and levels of significance are presented as (*) $p < 0.05$, (**) $p < 0.01$ and (***) $p < 0.001$.

dosage and length of exposure (1 μm and 5 min) of adrenaline were used in both 3D bioprinted samples and 2D samples (for representative image of 2D signals, see Supplementary Figure 3). Adrenaline treatment increased the beating rate in 3D bioprinted samples by 58 % (n = 5 recordings) from the average baseline beating rate of 12.6 BPM to the adrenaline-treated average beating rate of 24.6 BPM. Furthermore, 20 % of CPVT hiPSC-CMs had abnormal beating in the form of double peaks at baseline and adrenaline increased the abnormal beating behavior to 60 % of CPVT hiPSC-CMs (for representative image, see Fig. 6A) where Ca^{2+} fluctuated two peaks without reaching the baseline in between peaks. As a comparison, 40 % of the 2D cultured CPVT-CMs expressed abnormalities at baseline. The CPVT hiPSC-CMs were IF stained with Troponin T and CNX to visualize the elongated cell morphology and to detect the expression of CNX between adjacent hiPSC-CMs. Positive CNX staining was detected in CPVT hiPSC-CMs in both 2D controls and 3D bioprinted constructs (Fig. 6B and C).

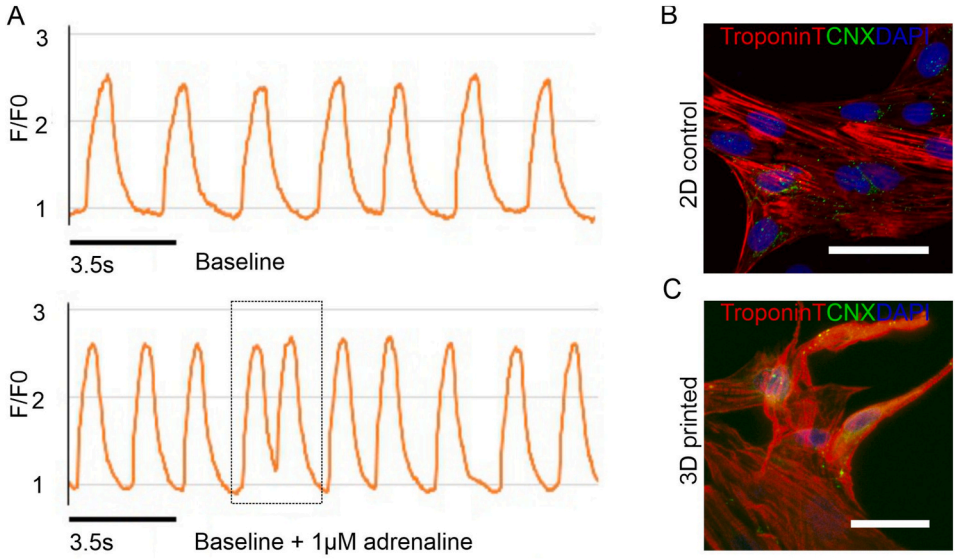

Fig. 6. 3D bioprinting of CPVT hiPSC-CMs for disease modeling. (A) Example of baseline Ca^{2+} signal (above) and adrenaline induced increase in beating rate with abnormal Ca^{2+} transit. (B) Confocal maximum intensity projection image of 2D cultured CPVT hiPSC-CMs IF stained against Troponin T (red), Connexin 43 (CNX) (green) and DAPI (blue). Scale bar 50 μm. (C) Confocal maximum intensity projection image of CPVT hiPSC-CMs in the 3D bioprinted *in vitro* model. Scale bar 25 μm, 40x objective. (For interpretation of the references to colour in this figure legend, the reader is referred to the Web version of this article.)

4. Discussion

Bioprinting has tremendous potential to create 3D cardiac models for disease modeling and *in vitro* drug screening by recapitulating the *in vivo* cell structure, geometry, and chemical and physiomechanical properties through a precise spatial control of cells and biomaterials [44]. hiPSCs have emerged as a key component of cardiac TE, cardiovascular disease mechanism modeling, and drug responses in human 3D tissue models [9]. To date, many advances have been made in using bioprinted hiPSC-CM constructs in this setting, such as the generation of myocardial infraction models [27,45] and vascularized cardiac tissue models [29,32]. However, no well-established 3D bioprinted cardiac tissue model currently exists that can be used as a basis for such studies. This study aimed to advance the development of cardiac 3D *in vitro* models by manufacturing 3D bioprinted hiPSC-derived cardiac constructs and assessing their functionality as well as applicability for drug screening and disease modeling. The ultimate goal was to demonstrate the feasibility of the 3D printing technology with hiPSC-CMs as well as show the proof-of-concept of the printed *in vitro* model with disease-specific cells.

GelMA has great potential for hydrogel-based bioinks due to its low cost, suitable biocompatibility, transparent structure, and tunable physical and chemical properties with photocrosslinking [46]. Here, we explored GelMA as the base for our bioink due to our extensive experience with gelatin, GelMA's unmodified form, as a basic growth substrate for hiPSC-CMs [13,41,47]. However, the 3D printing of pure GelMA bioinks is somewhat challenging because of its low viscosity at room temperature and even at higher temperatures. Moreover, the pure GelMA hydrogel does not fully satisfy the biological properties required in various tissues. Hence, we combined GelMA with human collagen I for improved printability and biocompatibility. Our GelMA and collagen I-based bioink exhibited good printability with extrusion printing. Previously, blends of photo-crosslinkable gelatin and collagen I have shown favorable rheological properties with drop-on-demand 3D bioprinting [48]. In our study, the developed bioink composition allowed high resolution printing using needle with inner diameter of 100 μm (32G), challenging the technological limits of extrusion-based bioprinting. Previously, 22G-30G nozzle diameters have been used for the extrusion printing of CMs and hiPSC-CMs [25,32,33,45].

In vitro modeling of a functional cardiac tissue by 3D bioprinting requires optimization of the mechanical properties of the bioink to resemble the native tissue and to provide optimal printing conditions to promote high cell viability, tissue formation and structural stability. Cardiac tissue is a mechanically complex tissue and hence, there is a great variability in the reported stiffness values in literature due to high variability in measurement settings. However, cardiac tissue is generally considered as a soft tissue, and tissue stiffening is a major contributor in several cardiac dysfunctions [49]. For example, Engler et al. reported a scale of native tissue stiffnesses, with $E < 10$ kPa in fetal, 10–15 kPa in adult, to 35–70 kPa in infarcted tissues (stiffness reported as Young's modulus) [50]. To determine mechanical properties of our bioink, we measured storage modulus (G′) of the GelMA and collagen I bioink by oscillatory from the acellular, bioprinted, and photocrosslinked constructs. Rheological results supported visual observation that bioprinted constructs were very soft ($G' = 0.15 \pm 0.018$ kPa) but also possessed high shape fidelity. Here, the 3D bioprinted constructs remained stable in cell culture conditions during the 20-day follow-up period, allowing the long-term culture of the printed structures which is a desirable property for an *in vitro* model. In addition, the mechanical properties of GelMA can be modified by choosing between the A or B type of gelatin, changing the ratio between methacrylic anhydride and gelatin, hydrogel concentration, and crosslinking density and conditions [51]. Pepelanova et al. were able to increase the stiffness (reported as G′) of GelMA hydrogel by 23%–73 % only by doubling the crosslinking UV intensity depending on the degree of functionalization of the material. This could be utilized in mimicking of stiffened cardiac tissue or specific stiffness values, making the model easily tunable. In future studies, the effects of cell-cell interactions and tissue maturation post-printing on the stiffness of the 3D bioprinted construct should be studied in more detail as these factors have been found to have profound affect to properties of the tissue during cardiac development [50]. Despite the good stability *in vitro*, the controlled degradation of the construct and the possibility to release encapsulated hiPSC-CMs for further analyses was easily done via enzymatic degradation. As both bioink components, gelatin and collagen I, contain enzymatically digestible sequences, accelerated enzymatic degradation can be used to provide information about enzyme involved in material remodeling and the degradation kinetics of the structure [51,52]. Overall, mechanical characterization of bioprinted constructs demonstrated high shape-fidelity of the constructs as well as excellent stability in cell culture and controlled degradation which are desirable properties for a versatile *in vitro* model [33,35,50–52].

A 3D culture environment is necessary for obtaining a proper CM phenotype and to mimic the native cardiac tissue [53]. Here, we observed elongated cell morphology and functionality with a well-developed Ca^{2+} handling system in the 3D bioprinted hiPSC-CMs in GelMA and collagen I bioink resembling CMs *in vivo* [54]. The hiPSC-CMs demonstrated good viability after 3D bioprinting and showed orientation according to the printed filament structure. Major morphological enhancements were observed in our 3D bioprinted hiPSC-CMs in IF stainings, including the elongated cell morphology, structural branching, and orientation of sarcomeres when compared to cells in 2D counterparts. These results indicate that the GelMA and collagen I bioink used in this study was cytocompatible with hiPSC-CMs and support cardiac tissue formation post-printing. Furthermore, collagen I is the most prominent ECM protein in the natural cardiac ECM [36]. Both bioink components, GelMA and collagen I are biocompatible and contain arginine-glycine-aspartic acid (RGD) sequences that improve cellular attachment [55]. Previously it has been shown that the addition of collagen I to GelMA has led to enhanced cell spreading with vascular tissue [48]. In addition to cardiomyocytes and cardiac ECM, native cardiac tissue is composed of endothelial cells (ECs), fibroblasts, leukocytes and vascular smooth muscle cells [56]. Previous studies have shown improvements in the hiPSC-CM morphology toward more physiological cardiomyocytes through methods such as co-culturing with other cell types like cardiac fibroblasts [57,58]. For these reasons we left the control hiPSC-CMs unpurified prior to bioprinting. Downside of this decision was overpowering of other cell types limiting culture time. In addition, previous bioprinting studies have utilized co-cultures of iPSC-CMs with cardiac fibroblasts [26,38] to demonstrate vascular formation with endothelial cells [27,32]. In the future, the controlled incorporation of endothelial cells and fibroblasts into the 3D bioprinted hiPSC-CM *in vitro* model should be explored to fully mimic the components and structure of the native cardiac tissue.

Imaging of the live bioprinted hiPSC-CMs is the most optimal method for studying functionality in 3D culture conditions. Ca^{2+} imaging is a method that enables functional analysis of CMs by monitoring intracellular Ca^{2+} fluxes and can be utilized in drug studies and understanding pathogenic mechanisms of cardiac diseases [34]. Ca^{2+} is a key factor in the excitation-contraction coupling of CMs, and abnormalities in Ca^{2+} handling can cause arrhythmias [34]. In this study, we demonstrated that the 3D bioprinting process did not hamper the functionality of the hiPSC-CMs, and Ca^{2+} imaging was convenient to perform for the hiPSC-CMs inside the 3D printed structure. Furthermore, 3D bioprinted hiPSC-CMs demonstrated significantly increased Ca^{2+} amplitudes and beating rates compared to their 2D cultured counterparts. An increase in the Ca^{2+} amplitude indicates stronger contractions and improved maturation [21,59]. Thus, these data indicate that the 3D bioprinting of hiPSC-CMs in GelMA and collagen I bioink supports the formation of functional cardiac constructs in 3D. In addition, the distribution of gap junctions is an important factor that regulates conduction velocity and indicates maturation level of the CMs. The gap junction protein connexin 43 has been shown to be circumferentially distributed

during fetal life, and, as the postnatal rodent heart matures, these proteins become progressively concentrated into intercalated disks at the ends of the cells [60]. In our study, the 3D bioprinted hiPSC-CMs demonstrated concentrated connexin-43 expression between adjacent cells, demonstrating the formation of gap junctions in the 3D bioprinted model. However, also cells with more immature and more circumferentially distributed connexin were seen in the printed structures indicating partly less maturated phenotype. Overall, immature phenotype of the hiPSC-CMs has raised a lot of discussion in the field. Methods to improve and study maturity has been covered in many recent publications [60–63]. To fully harness the potential of 3D bioprinted hiPSC-CM model, more research is needed to evaluate maturation status of the hiPSC-CMs growing in the 3D bioprinted model.

Cardiac TE searches for solutions to produce the physiological tissue environment to investigate cardiac function and biology under normal and also pathological conditions [9]. Here, we explored the feasibility of our 3D bioprinted model with patient specific hiPSC-CMs carrying the RyR2 gene mutation for CPVT. The bioprinted hiPSC-CMs with the mutation demonstrated their phenotypic beating abnormalities [11] in 3D bioprinted structures. Adrenaline induced increments in beating rates in CPVT hiPSC-CMs, leading to arrhythmias in 60 % of the studied cells. This increased susceptibility to arrhythmias is in the similar range observed in our earlier studies with the same mutant line in the 2D condition [11]. Moreover, induced increase in beating rate and resulting Ca^{2+} transient abnormalities were in line with the results from Goldfracht et al. who presented similar results from CPVT hiPSC-CMs grown in engineered heart tissues [64]. Furthermore, adrenaline effected to beating rate of the CPVT hiPSC-CMs as rapidly in 3D structures as in 2D cultures, indicating that there was no material-related delay in drug diffusion to the hiPSC-CMs growing inside the 3D structure. In the present study, CPVT hiPSC-CMs in 2D controls expressed more abnormalities at baseline than the CPVT hiPSC-CMs in 3D bioprinted *in vitro* models. This indicates better correspondence of 3D cultured CPVT-CMs to pathognomonic feature of exercise-induced beating abnormalities which are normally lacking from the resting heart rhythm [65,66]. As the 3D culturing is known to improve maturity of cardiomyocytes and hence to promote electrophysical maturation [67], hiPSC CPVT-CMs cultured in 3D express more physiological correspondence than their 2D cultured counterparts. In future studies, antiarrhythmic drug components should be tested to validate further the advantages of this 3D bioprinted model in drug screening and discovery. To the best of our knowledge, this study is the first to demonstrate the feasibility of 3D bioprinting of CPVT hiPSC-CMs. Altogether, these results indicate that the developed 3D bioprinted hiPSC-CM *in vitro* model has great potential for disease modeling in cardiac TE.

5. Conclusions

In this study, we developed a 3D *in vitro* model for cardiac TE using hiPSC-CMs, GelMA, and collagen I-based bioink and extrusion-ased 3D bioprinting. The developed 3D bioprinted constructs showed good structural and mechanical stability in promoting long-term *in vitro* cultures. 3D bioprinted hiPSC-CMs showed good cell viability, elongated cell morphology and functionality. Moreover, the hiPSC-CMs demonstrated more native cell morphology in 3D bioprinted structures compared to 2D cultures. Finally, we demonstrated the feasibility of the model for disease modeling by 3D bioprinting patient-specific hiPSC-CMs. The 3D bioprinted patient-specific *in vitro* model showed improved disease phenotype of CPVT compared to 2D cultures. Thus, developed 3D bioprinted hiPSC-CM model shows great promise for future cardiac TE and advances the translation of cardiac 3D models toward functional and patient-derived *in vitro* models for disease modeling and drug screening.

Ethical issues

This study was carried out under the ethical approval by the Ethics Committee of Pirkanmaa Hospital District regarding culturing and differentiating of human iPSC lines (R08070). Written informed consent was obtained from all the participants.

Funding

This study was supported by the Academy of Finland (324082), Sigrid Juselius Foundation, Finnish Cardiovascular Research Foundation.

CRediT authorship contribution statement

Henna Lappi: Methodology, Investigation, Formal analysis, Writing – original draft, Writing – review & editing, Visualization. **Maija Kauppila:** Methodology, Investigation, Writing – original draft. **Katriina Aalto-Setälä:** Resources, Supervision, Writing – review & editing. **Anni Mörö:** Methodology, Resources, Supervision, Writing – original draft, Writing – review & editing.

Declaration of competing interest

The authors declare that they have no known competing financial interests or personal relationships that could have appeared to influence the work reported in this paper.

Data availability

Data will be made available on request.

Acknowledgements

Tampere University Imaging and CellTech Cores are thanked for providing equipment for the study.

Appendix A. Supplementary data

Supplementary data to this article can be found online at https://doi.org/10.1016/j.bprint.2023.e00313.

References

[1] World Health Organization. WHO reveals leading causes of death and disability worldwide: 2000-2019 2020. https://www.who.int/news/item/09-12-2020-who-reveals-leading-causes-of-death-and-disability-worldwide-2000-2019..
[2] L. Sala, M. Bellin, C.L. Mummery, Integrating cardiomyocytes from human pluripotent stem cells in safety pharmacology: has the time come? Br. J. Pharmacol. 174 (2017) 3749–3765, https://doi.org/10.1111/bph.13577.
[3] I.J. Onakpoya, C.J. Heneghan, J.K. Aronson, Post-marketing withdrawal of 462 medicinal products because of adverse drug reactions: a systematic review of the world literature, BMC Med. 14 (2016) 10, https://doi.org/10.1186/s12916-016-0553-2.
[4] F.P. Kreutzer, A. Meinecke, K. Schmidt, J. Fiedler, T. Thum, Alternative strategies in cardiac preclinical research and new clinical trial formats, Cardiovasc. Res. 118 (2022) 746–762, https://doi.org/10.1093/cvr/cvab075.
[5] C. Riehle, J. Bauersachs, Small animal models of heart failure, Cardiovasc. Res. 115 (2019) 1838–1849, https://doi.org/10.1093/cvr/cvz161.
[6] N. Milani-Nejad, P.M.L. Janssen, Small and large animal models in cardiac contraction research: advantages and disadvantages, Pharmacol. Ther. 141 (2014) 235–249, https://doi.org/10.1016/j.pharmthera.2013.10.007.
[7] L. Sala, M. Bellin, C.L. Mummery, Integrating cardiomyocytes from human pluripotent stem cells in safety pharmacology: has the time come? Br. J. Pharmacol. 174 (2017) 3749–3765, https://doi.org/10.1111/bph.13577.
[8] M. Ojala, C. Prajapati, R.-P. Pölönen, K. Rajala, M. Pekkanen-Mattila, J. Rasku, et al., Mutation-specific phenotypes in hiPSC-derived cardiomyocytes carrying either myosin-binding protein C or α -tropomyosin mutation for hypertrophic cardiomyopathy, Stem Cell. Int. 2016 (2016) 1–16, https://doi.org/10.1155/2016/1684792.

[9] S. Cho, C. Lee, M.A. Skylar-Scott, S.C. Heilshorn, J.C. Wu, Reconstructing the heart using iPSCs: engineering strategies and applications, J. Mol. Cell. Cardiol. 157 (2021) 56–65, https://doi.org/10.1016/j.yjmcc.2021.04.006.

[10] M. Alonzo, S. AnilKumar, B. Roman, N. Tasnim, B. Joddar, 3D Bioprinting of cardiac tissue and cardiac stem cell therapy, Transl. Res. 211 (2019) 64–83, https://doi.org/10.1016/j.trsl.2019.04.004.

[11] K. Penttinen, H. Swan, S. Vanninen, J. Paavola, A.M. Lahtinen, K. Kontula, et al., Antiarrhythmic effects of dantrolene in patients with catecholaminergic polymorphic ventricular tachycardia and replication of the responses using iPSC models, PLoS One 10 (2015) 1–17, https://doi.org/10.1371/journal.pone.0125366.

[12] M. Ojala, C. Prajapati, R.-P. Pölönen, K. Rajala, M. Pekkanen-Mattila, J. Rasku, et al., Mutation-specific phenotypes in hiPSC-derived cardiomyocytes carrying either myosin-binding protein C or α -tropomyosin mutation for hypertrophic cardiomyopathy, Stem Cell. Int. 2016 (2016) 1–16, https://doi.org/10.1155/2016/1684792.

[13] A.L. Kiviaho, A. Ahola, K. Larsson, K. Penttinen, H. Swan, M. Pekkanen-Mattila, et al., Distinct electrophysiological and mechanical beating phenotypes of long QT syndrome type 1-specific cardiomyocytes carrying different mutations, IJC Heart Vasc 8 (2015) 19–31, https://doi.org/10.1016/j.ijcha.2015.04.008.

[14] A.L. Lahti, V.J. Kujala, H. Chapman, A.-P. Koivisto, M. Pekkanen-Mattila, E. Kerkelä, et al., Model for long QT syndrome type 2 using human iPS cells demonstrates arrhythmogenic characteristics in cell culture, Dis Model Mech 5 (2012) 220–230, https://doi.org/10.1242/dmm.008409.

[15] L.A. Macqueen, S.P. Sheehy, C.O. Chantre, J.F. Zimmerman, F.S. Pasqualini, X. Liu, et al., A tissue-engineered scale model of the heart ventricle, Nat. Biomed. Eng. 2 (2018) 930–941, https://doi.org/10.1038/s41551-018-0271-5.

[16] Y. Guo, W.T. Pu, Cardiomyocyte maturation, Circ. Res. 126 (2020) 1086–1106, https://doi.org/10.1161/CIRCRESAHA.119.315862.

[17] M. Tiburcy, J.E. Hudson, P. Balfanz, S. Schlick, T. Meyer, M.L.C. Liao, et al., Defined engineered human myocardium with advanced maturation for applications in heart failure modeling and repair, Circulation 135 (2017) 1832–1847, https://doi.org/10.1161/CIRCULATIONAHA.116.024145.

[18] S. Schaaf, A. Shibamiya, M. Mewe, A. Eder, A. Stöhr, M.N. Hirt, et al., Human engineered heart tissue as a versatile tool in basic research and preclinical toxicology, PLoS One 6 (2011), e26397, https://doi.org/10.1371/journal.pone.0026397.

[19] P. Abadi, J. Garbern, S. Behzadi, M. Hill, J. Tresback, T. Heydari, et al., Engineering of mature human induced pluripotent stem cell-derived cardiomyocytes using substrates with multiscale topography, Adv. Funct. Mater. 28 (2018), https://doi.org/10.1002/adfm.201707378.

[20] C. Correia, A. Koshkin, P. Duarte, D. Hu, M. Carido, M.J. Sebastião, et al., 3D aggregate culture improves metabolic maturation of human pluripotent stem cell derived cardiomyocytes, Biotechnol. Bioeng. 115 (2018) 630–644, https://doi.org/10.1002/bit.26504.

[21] C. Sacchetto, L. Vitiello, L.J. de Windt, A. Rampazzo, M. Calore, Modeling cardiovascular diseases with hiPSC-derived cardiomyocytes in 2D and 3D cultures, Int. J. Mol. Sci. 21 (2020) 3404, https://doi.org/10.3390/ijms21093404.

[22] K. Willson, A. Atala, J.J. Yoo, Bioprinting Au natural: the biologics of bioinks, Biomolecules 11 (2021) 1593, https://doi.org/10.3390/biom11111593.

[23] Y. Tsukamoto, T. Akagi, M. Akashi, Vascularized cardiac tissue construction with orientation by layer-by-layer method and 3D printer, Sci. Rep. 10 (2020) 5484, https://doi.org/10.1038/s41598-020-59371-y.

[24] P. Abadi, J. Garbern, S. Behzadi, M. Hill, J. Tresback, T. Heydari, et al., Engineering of mature human induced pluripotent stem cell-derived cardiomyocytes using substrates with multiscale topography, Adv. Funct. Mater. 28 (2018), https://doi.org/10.1002/adfm.201707378.

[25] B. Kang, Y. Park, D.G. Hwang, D. Kim, U. Yong, K.S. Lim, et al., Facile bioprinting process for fabricating size-controllable functional microtissues using light-activated decellularized extracellular matrix-based bioinks, Adv Mater Technol 7 (2022), 2100947, https://doi.org/10.1002/admt.202100947.

[26] A.C. Daly, M.D. Davidson, J.A. Burdick, 3D bioprinting of high cell-density heterogeneous tissue models through spheroid fusion within self-healing hydrogels, Nat. Commun. 12 (2021) 753, https://doi.org/10.1038/s41467-021-21029-2.

[27] E. Yeung, T. Fukunishi, Y. Bai, D. Bedja, I. Pitaktong, G. Mattson, et al., Cardiac regeneration using human-induced pluripotent stem cell-derived biomaterial-free 3D-bioprinted cardiac patch in vivo, J Tissue Eng Regen Med 13 (2019) 2031–2039, https://doi.org/10.1002/term.2954.

[28] C.S. Ong, T. Fukunishi, H. Zhang, C.Y. Huang, A. Nashed, A. Blazeski, et al., Biomaterial-free three-dimensional bioprinting of cardiac tissue using human induced pluripotent stem cell derived cardiomyocytes, Sci. Rep. 7 (2017) 2–12, https://doi.org/10.1038/s41598-017-05018-4.

[29] Y.S. Zhang, A. Arneri, S. Bersini, S.-R. Shin, K. Zhu, Z. Goli-Malekabadi, et al., Bioprinting 3D microfibrous scaffolds for engineering endothelialized myocardium and heart-on-a-chip, Biomaterials 110 (2016) 45–59, https://doi.org/10.1016/j.biomaterials.2016.09.003.

[30] S. Anil Kumar, M. Alonzo, S.C. Allen, L. Abelseth, V. Thakur, J. Akimoto, et al., A visible light-cross-linkable, fibrin-gelatin-based bioprinted construct with human cardiomyocytes and fibroblasts, ACS Biomater. Sci. Eng. 5 (2019) 4551–4563, https://doi.org/10.1021/acsbiomaterials.9b00505.

[31] K.L. Miller, Y. Xiang, C. Yu, J. Pustelnik, J. Wu, X. Ma, et al., Rapid 3D BioPrinting of a human iPSC-derived cardiac micro-tissue for high-throughput drug testing, Organs—Chip 3 (2021), 100007, https://doi.org/10.1016/j.ooc.2021.100007.

[32] N. Noor, A. Shapira, R. Edri, I. Gal, L. Wertheim, T. Dvir, 3D printing of personalized thick and perfusable cardiac patches and hearts, Adv. Sci. 6 (2019), https://doi.org/10.1002/advs.201900344.

[33] Y.J. Shin, R.T. Shafranek, J.H. Tsui, J. Walcott, A. Nelson, D.H. Kim, 3D bioprinting of mechanically tuned bioinks derived from cardiac decellularized extracellular matrix, Acta Biomater. 119 (2021) 75–88, https://doi.org/10.1016/j.actbio.2020.11.006.

[34] H. Sutanto, A. Lyon, J. Lumens, U. Schotten, D. Dobrev, J. Heijman, Cardiomyocyte calcium handling in health and disease: insights from in vitro and in silico studies, Prog. Biophys. Mol. Biol. 157 (2020) 54–75, https://doi.org/10.1016/j.pbiomolbio.2020.02.008.

[35] P.S. Gungor-Ozkerim, I. Inci, Y.S. Zhang, A. Khademhosseini, M.R. Dokmeci, Bioinks for 3D bioprinting: an overview, Biomater. Sci. 6 (2018) 915–946, https://doi.org/10.1039/c7bm00765e.

[36] H. Li, M. Bao, Y. Nie, Extracellular matrix–based biomaterials for cardiac regeneration and repair, Heart Fail. Rev. (2020), https://doi.org/10.1007/s10741-020-09953-9.

[37] B.D. Fairbanks, M.P. Schwartz, C.N. Bowman, K.S. Anseth, Photoinitiated polymerization of PEG-diacrylate with lithium phenyl-2,4,6-trimethylbenzoylphosphinate: polymerization rate and cytocompatibility, Biomaterials 30 (2009) 6702–6707, https://doi.org/10.1016/j.biomaterials.2009.08.055.

[38] K.L. Miller, Y. Xiang, C. Yu, J. Pustelnik, J. Wu, X. Ma, et al., Rapid 3D BioPrinting of a human iPSC-derived cardiac micro-tissue for high-throughput drug testing, Organs—Chip 3 (2021), 100007, https://doi.org/10.1016/j.ooc.2021.100007.

[39] M. Tiburcy, J.E. Hudson, P. Balfanz, S. Schlick, T. Meyer, M.-L. Chang Liao, et al., Defined engineered human myocardium with advanced maturation for applications in heart failure modeling and repair, Circulation 135 (2017) 1832–1847, https://doi.org/10.1161/CIRCULATIONAHA.116.024145.

[40] R. Maria Cherian, C. Prajapati, K. Penttinen, M. Häkli, J.T. Koivisto, M. Pekkanen-Mattila, et al., Fluorescent hiPSC-derived MYH6-mScarlet cardiomyocytes for real-time tracking, imaging, and cardiotoxicity assays, Cell Biol. Toxicol. (2022), https://doi.org/10.1007/s10565-022-09742-0.

[41] C. Prajapati, M. Ojala, H. Lappi, K. Aalto-Setälä, M. Pekkanen-Mattila, Electrophysiological evaluation of human induced pluripotent stem cell-derived cardiomyocytes obtained by different methods, Stem Cell Res. 51 (2021), 102176, https://doi.org/10.1016/j.scr.2021.102176.

[42] C. Mummery, D. Ward-van Oostwaard, P. Doevendans, R. Spijker, S. van den Brink, R. Hassink, et al., Differentiation of human embryonic stem cells to cardiomyocytes, Circulation 107 (2003) 2733–2740, https://doi.org/10.1161/01.CIR.0000068356.38592.68.

[43] E. Wershof, D. Park, D. Barry, R. Jenkins, A. Rullan, A. Wilkins, et al., A Fiji macro for quantifying pattern in extracellular matrix, Life Sci. Alliance (2021), https://doi.org/10.26508/lsa.202000880.

[44] J.B. Hu, M.L. Tomov, J.W. Buikema, C. Chen, M. Mahmoudi, S.M. Wu, et al., Cardiovascular tissue bioprinting: physical and chemical processes, Appl. Phys. Rev. 5 (2018), 041106, https://doi.org/10.1063/1.5048807.

[45] G. Basara, S.G. Ozcebe, B.W. Ellis, P. Zorlutuna, Tunable human myocardium derived decellularized extracellular matrix for 3D bioprinting and cardiac tissue engineering, Gels 7 (2021) 70, https://doi.org/10.3390/gels7020070.

[46] N. Rajabi, A. Rezaei, M. Kharaziha, H.R. Bakhsheshi-Rad, H. Luo, S. RamaKrishna, et al., Recent advances on bioprinted gelatin methacrylate-based hydrogels for tissue repair, Tissue Eng. 27 (2021) 679–702, https://doi.org/10.1089/ten.tea.2020.0350.

[47] M. Häkli, J. Kreutzer, A.J. Mäki, H. Välimäki, H. Lappi, H. Huhtala, et al., Human induced pluripotent stem cell-based platform for modeling cardiac ischemia, Sci. Rep. 11 (2021) 1–13, https://doi.org/10.1038/s41598-021-83740-w.

[48] H. Stratesteffen, M. Köpf, F. Kreimendahl, A. Blaeser, S. Jockenhoevel, H. Fischer, GelMA-collagen blends enable drop-on-demand 3D printablility and promote angiogenesis, Biofabrication 9 (2017), 045002, https://doi.org/10.1088/1758-5090/aa857c.

[49] R. Emig, C.M. Zgierski-Johnston, V. Timmermann, A.J. Taberner, M.P. Nash, P. Kohl, et al., Passive myocardial mechanical properties: meaning, measurement, models, Biophys Rev 13 (2021) 587–610, https://doi.org/10.1007/s12551-021-00838-1.

[50] A.J. Engler, C. Carag-Krieger, C.P. Johnson, M. Raab, H.-Y. Tang, D.W. Speicher, et al., Embryonic cardiomyocytes beat best on a matrix with heart-like elasticity: scar-like rigidity inhibits beating, J. Cell Sci. 121 (2008) 3794–3802, https://doi.org/10.1242/jcs.029678.

[51] I. Pepelanova, K. Kruppa, T. Scheper, A. Lavrentieva, Gelatin-methacryloyl (GelMA) hydrogels with defined degree of functionalization as a versatile toolkit for 3D cell culture and extrusion bioprinting, Bioengineering 5 (2018), https://doi.org/10.3390/bioengineering5030055.

[52] M. Zhu, Y. Wang, G. Ferracci, J. Zheng, N.J. Cho, B.H. Lee, Gelatin methacryloyl and its hydrogels with an exceptional degree of controllability and batch-to-batch consistency, Sci. Rep. 9 (2019) 1–13, https://doi.org/10.1038/s41598-019-42186-x.

[53] F. Varzideh, P. Mone, G. Santulli, Bioengineering strategies to create 3D cardiac constructs from human induced pluripotent stem cells, Bioengineering 9 (2022) 168, https://doi.org/10.3390/bioengineering9040168.

[54] J. Li, Y. Hua, S. Miyagawa, J. Zhang, L. Li, L. Liu, et al., HiPSC-derived cardiac tissue for disease modeling and drug discovery, Int. J. Mol. Sci. 21 (2020) 1–32, https://doi.org/10.3390/ijms21238893.

[55] K. Yue, G. Trujillo-de Santiago, M.M. Alvarez, A. Tamayol, N. Annabi, A. Khademhosseini, Synthesis, properties, and biomedical applications of gelatin

methacryloyl (GelMA) hydrogels, Biomaterials 73 (2015) 254–271, https://doi.org/10.1016/j.biomaterials.2015.08.045.
[56] C. Liu, A. Oikonomopoulos, N. Sayed, J.C. Wu, Modeling human diseases with induced pluripotent stem cells: from 2D to 3D and beyond, Dev Camb 145 (2018) 1–6, https://doi.org/10.1242/dev.156166.
[57] P. Beauchamp, C.B. Jackson, L.C. Ozhathil, I. Agarkova, C.L. Galindo, D.B. Sawyer, et al., 3D Co-culture of hiPSC-derived cardiomyocytes with cardiac fibroblasts improves tissue-like features of cardiac spheroids, Front. Mol. Biosci. 7 (2020), https://doi.org/10.3389/fmolb.2020.00014.
[58] H. Saini, A. Navaei, A. Van Putten, M. Nikkhah, 3D cardiac microtissues encapsulated with the Co-culture of cardiomyocytes and cardiac fibroblasts, Adv. Healthcare Mater. 4 (2015) 1961–1971, https://doi.org/10.1002/adhm.201500331.
[59] M. Cagalinec, I. Waczulíková, O. Uličná, D. Chorvat, Morphology and contractility of cardiac myocytes in early stages of streptozotocin-induced diabetes mellitus in rats, Physiol. Res. (2013) 489–501, https://doi.org/10.33549/physiolres.932467.
[60] X. Yang, L. Pabon, C.E. Murry, Engineering adolescence: maturation of human pluripotent stem cell-derived cardiomyocytes, Circ. Res. 114 (2014) 511–523, https://doi.org/10.1161/CIRCRESAHA.114.300558.
[61] R. Ahmed, T. Anzai, N. Chanthra, H. Uosaki, A brief review of current maturation methods for human induced pluripotent stem cells-derived cardiomyocytes, Front. Cell Dev. Biol. (2020), https://doi.org/10.3389/fcell.2020.00178.
[62] G. Maroli, T. Braun, The long and winding road of cardiomyocyte maturation, Cardiovasc. Res. (2021), https://doi.org/10.1093/cvr/cvaa159.
[63] M.-T. Zhao, S. Ye, J. Su, V. Garg, Cardiomyocyte proliferation and maturation: two sides of the same coin for heart regeneration, Front. Cell Dev. Biol. (2020), https://doi.org/10.3389/fcell.2020.594226.
[64] I. Goldfracht, Y. Efraim, R. Shinnawi, E. Kovalev, I. Huber, A. Gepstein, et al., Engineered heart tissue models from hiPSC-derived cardiomyocytes and cardiac ECM for disease modeling and drug testing applications, Acta Biomater. 92 (2019) 145–159, https://doi.org/10.1016/j.actbio.2019.05.016.
[65] A.V. Postma, Catecholaminergic polymorphic ventricular tachycardia: RYR2 mutations, bradycardia, and follow up of the patients, J. Med. Genet. 42 (2005) 863–870, https://doi.org/10.1136/jmg.2004.028993.
[66] C. Van Der Werf, A.A.M. Wilde, Catecholaminergic polymorphic ventricular tachycardia: from bench to bedside, Heart 99 (2013) 497–504, https://doi.org/10.1136/heartjnl-2012-302033.
[67] P. Wu, G. Deng, X. Sai, H. Guo, H. Huang, P. Zhu, Maturation strategies and limitations of induced pluripotent stem cell-derived cardiomyocytes, Biosci. Rep. (2021), https://doi.org/10.1042/BSR20200833.